Assessment of high-efficacy agonism in synthetic cannabinoid receptor agonists containing l-*tert*-leucinate

Christopher Lucaj, Soo Jung Oh, Charlotte Pitha, Jordan Davis, Hideaki Yano*

Department of Pharmaceutical Sciences, School of Pharmacy and Pharmaceutical Sciences, Bouvé College of Health Sciences, Center for Drug Discovery, Northeastern University, Boston, Massachusetts 02115, United States

*h.yano@northeastern.edu

Abstract

Synthetic cannabinoid receptor agonists (SCRAs) represent a class of new psychoactive substances that pose great health risks attributed to their wide-ranging and severe adverse effects. Recent evidence has shown that SCRAs with key moieties can confer superagonism, yet this phenomenon is still not well understood. Here we report structure-activity relationships (SARs) of modular SCRAs contributing to superagonism by comparing eight compounds differing by their head moiety (l-valinate vs. l-*tert*-leucinate), core moiety (indole vs. indazole), and tail moiety (5-fluoropentyl vs. 4-fluorobenzyl) through different modes of bioluminescence resonance energy transfer (BRET) assays. We found that the l-*tert*-leucinate head moiety and indazole core moiety conferred superagonism across multiple $G\alpha_{i/o}$ proteins and β-arrestin-2. After generating the cannabinoid type 1 receptor (CB1R) mutant constructs, we found that transmembrane 2 (TM2) interactions to the head moiety of tested SCRAs at F170, F174, F177, and H178 are key to eliciting activity. Finally, we found that l-*tert*-leucinate SCRAs confer a high-efficacy response in *ex vivo* slice electrophysiology.

1. Introduction

The severe adverse effects observed with SCRA use are distinct from those of delta-9-tetrahydrocannabinol (THC), the active compound found in *Cannabis sativa* [1-4]. Due to the aminoalkyl-heterocycle scaffolds of SCRAs, drugs can be made through iterative modular design, resulting in greatly increased efficacy and potency and leading to their illicit use, as noted by the >100 novel SCRAs identified by the United Nations Office on Drugs and Crime every year since 2013 [5]. MMB-FUBINACA, one of these SCRAs, was responsible for a well-publicized case of SCRA intoxication that occurred in 2016 when thirty-three people exhibiting “zombie-like” cataleptic behavior [6]. In a separate clinical

case, patients experienced extreme agitation, aggressiveness, and seizures after using another SCRA ADB-PINACA [3]. Compared to chronic cannabis use, cessation of SCRA use can lead to more severe withdrawal symptoms, with less frequency and volume of consumption [7, 8]. Although rare, SCRA overdose lethality has been reported, whereas that has not been reported with cannabis use [9-12].

With high affinity, SCRAs bind CB1R, a highly expressed G-protein coupled receptor (GPCR) in the brain and CNS [1, 13]. CB1R plays a crucial role in downregulating neurotransmitter release, primarily through $G\alpha_{i/o}$ signaling pathways initiated by retrograde signaling at synaptic terminals [14, 15]. Upon G-protein activation, voltage-gated Ca^{2+} channels are inhibited and G-protein-gated inward rectifying K^+ channels are activated, resulting in pre-synaptic hyperpolarization [14, 16]. Peripherally, the receptor also plays an important role in cardiovascular function as well as energy metabolism [17-19]. CB1R expression and function in multiple systems are complemented by the differential expression of the $G\alpha_{i/o}$ protein subfamily, consisting of ubiquitously ($G\alpha_{i1}$, $G\alpha_{i2}$, $G\alpha_{i3}$) and neuronally ($G\alpha_{oA}$, $G\alpha_{oB}$, $G\alpha_{z}$) expressed inhibitory G-proteins [20-23]. Pharmacological studies have characterized a number of SCRAs based on CB1R-mediated cAMP inhibition as well as β-arrestin internalization [24-27]. SCRA-induced G-protein signaling within the subfamily of $G\alpha_{i/o}$ proteins, however, has only been investigated very recently [26, 28, 29]. Though these studies found SCRAs to show little functional selectivity or bias, a thorough comparison of moieties among structural analogs has not been attempted by using rigorous proximity assay approaches.

With the increasing number of newly reported chemical structures, SCRA pharmacology has been assessed by potency and efficacy of conventional functional assays. Indeed, SARs of these chemical structures, composed of three key moieties (head, core, and tail), have led to a characterization of SCRAs as “high efficacy” agonists [6, 10, 24, 25]. However, assays that measure activity downstream of receptor-transducer interactions may be affected by signal amplification, leading to an inaccurate assessment of reduced efficacy and increased potency [30]. This limitation warrants the incorporation of a rigorous study design that is less affected by signal amplification. Recently, we investigated the SAR between two compounds, 5F-MMB-PICA (M-PC) and 5F-MDMB-PICA (D-PC), that differed in a single methyl group in the “head” moiety [31]. D-PC, with an l-*tert*-leucinate head moiety, was shown to act as a “superagonist”, an agonist that has greater efficacy than that of the endogenous ligand, while M-PC acted as a full agonist [30, 31]. Notably, molecular dynamics simulations between these drugs revealed different levels of interaction with key residues in the extracellular TM2 domain, a region recently reported to be critical in activation of CB1R [31-34]. Although we found a SCRA that elicits superagonism, an understanding of what drives CB1R superagonism is still limited.

In the current study, we further explore differences in SCRA moieties to uncover CB1R superagonism based on differences in “head,” “core,” and “tail” moieties. With a panel of

eight compounds, we use different modes of BRET assays to assess the efficacy, bias, and functional selectivity of these compounds. We then introduced point mutations in TM2 residues of CB1R to reveal key interactions with the head moiety l-*tert*-leucinate. Finally, we measured the effects of SCRAs on CB1R-mediated inhibition of glutamate release in the hippocampus through *ex vivo* slice electrophysiology.

2. Materials and Methods

2.1 Mammalian Cell Culture

All *in vitro* assays are performed in human embryonic kidney 293 T (HEK-293T) cells cultured in Dulbecco's Modified Eagle Medium (DMEM) supplemented with 10% fetal bovine serum (FBS), 1% penicillin/streptomycin, and 2 mM L-glutamine and incubated at 37°C and 5% CO_2. HEK-293T cells are cultured in 10-cm plates at a high cell density of 375,000 cells/ml (3 x 10^6 cells/8 ml) twenty-four hours prior to transfection. Cells are maintained using aseptic technique and are used in pharmacological assays within 5-30 passages.

2.2 Animals

C57Bl/6 mice are maintained in a vivarium provided by the Department of Laboratory Animal Medicine of Northeastern University. All experimental procedures performed on mice are in accordance with protocols approved by the Institutional Animal Care and Use Committee at Northeastern University.

2.3 Compounds & Plasmid Constructs

All CB1R ligands used in this study are purchased or acquired from Cayman Chemical (Ann Arbor, Michigan) or NIDA Drug Supply Program (Rockville, Maryland). The ligands are dissolved in DMSO to a stock concentration of 10 mM. All DNA constructs are generated in pcDNA3 plasmid vectors. Alanine substitutions of *CNR1*-containing plasmid constructs were generated using the Quickchange Site-Directed Mutagenesis Kit (Agilent) and the following primers:
F170A forward primer 5' – TGGGGAGTGTCATTGCTGTCTACAGCTTCAT – 3',
reverse primer 5' – ATGAAGCTGTAGACAGCAATGACACTCCCCA – 3';
S173A forward primer 5' – TCATTTTTGTCTACGCCTTCATTGACTTCCA – 3',
reverse primer 5' – TGGAAGTCAATGAAGGCGTAGACAAAAATGA 3';
F174A forward primer 5' – ACAGCTTCATTGACGCCCACGTGTTCCACC – 3',
reverse primer 5' – GGTGGAACACGTGGGCGTCAATGAAGCTGT – 3';
F177A forward primer 5' – TTTTTGTCTACAGCGCCATTGACTTCCACG – 3',
reverse primer 5' – CGTGGAAGTCAATGGCGCTGTAGACAAAAA – 3';
H178A forward primer 5' – GCTTCATTGACTTCGCCGTGTTCCACCGCA – 3',
reverse primer 5' – TGCGGTGGAACACGGCGAAGTCAATGAAGC – 3'.

2.4 Bioluminescence Resonance Energy Transfer (BRET) receptor function assays

2.4.1 General BRET methodology

BRET assays described below contain variations in DNA constructs transfected and in method of experimentation. Consistent with all experiments is a pre-incubation of 5-15 µg DNA (per 10-cm plate, DNA amounts vary by experiment) with 30 µg/cell plate linear polyethyleneimine (PEI) in serum-free DMEM twenty minutes before addition to cells. After overnight treatment, media is fully replaced with fresh, supplemented DMEM. After 48 hours of transfection, cells are washed with phosphate-buffered saline (PBS), harvested, and resuspended in PBS containing 0.1% glucose, 200 µM sodium bisulfite and 1 mg/mL fatty acid-free bovine serum albumin (BSA), which serves as a drug stabilizer. Cells are evenly distributed amongst wells in white flat-bottom 96 well plates. On the day of experiment, serially diluted drugs are transferred to cells three minutes after 5 µM coelenterazine H incubation. Luminescence and fluorescence values are recorded 10 minutes after drug treatment in a PheraStar FSX plate reader (bioluminescence at 480 nm, fluorescence at 530 nm). BRET ratio is calculated based on the measurement of fluorescence divided by that of luminescence. BRET ratios are then normalized to the basal BRET ratio calculated by the non-linear regression generated by GraphPad Prism 10.

2.4.2 G-protein/β-arrestin engagement

Plasmid DNA in engagement BRET assays have been reported [31] as follows: CB1R tagged with *Renilla* luciferase 8 (CB1R-RLuc), $G\alpha_{i1}$ tagged with Venus ($G\alpha_{i1}V$), $G\beta_1$, and $G\gamma_2$. For β-arrestin engagement, β-arrestin-2 tagged with Venus (βArr2V) and G-protein coupled receptor kinase 2 (GRK2) are used.

2.4.3 G-protein activation

Plasmid DNA in activation BRET assays have been reported [35, 36] as follows: Untagged CB1R, Gα tagged with *Renilla* luciferase 8 ($G\alpha_{i1}$-RLuc, $G\alpha_{i2}$-RLuc, $G\alpha_{i3}$-RLuc, $G\alpha_{oA}$-RLuc, $G\alpha_{oB}$-RLuc, or $G\alpha_{z}$-RLuc), $G\beta_1$, and $G\gamma_2$ tagged with Venus ($G\gamma_2V$).

2.5 Ex vivo slice electrophysiology

Young adult mice (8-20 weeks old) anesthetized with isoflurane were intracardially perfused with slicing artificial cerebral spinal fluid (slicing ACSF) containing (in mM): 92 NMDG, 20 HEPES, 25 glucose, 30 NaHCO3, 1.2 NaH2PO4, 2.5 KCl, 5 sodium ascorbate, 3 sodium pyruvate, 2 thiourea, 10 MgSO4, 0.5 CaCl2, 300–310 mOsm, at pH 7.3–7.4. After decapitation, the mouse brain is fixed to a stage, submerged in cold slicing ACSF saturated with 95% O2 and 5% CO2 (carbogen), and sectioned in a para-sagittal manner at 300 µm using a vibratome. Brain slices are transferred to 37°C slicing ACSF for seven minutes, then transferred to room temperature holding ACSF saturated with

carbogen containing (in mM): 92 NaCl, 20 HEPES, 25 glucose, 30 NaHCO3, 1.2 NaH2PO4, 2.5 KCl, 5 sodium ascorbate, 3 sodium pyruvate, 2 thiourea, 1 MgSO4, 2 CaCl2, 300–310 mOsm, at pH 7.3–7.4. Slices are maintained in holding ACSF for 1.5 to 2 hours prior to experimentation. Brain slices are transferred into a recording chamber filled with recording ACSF that contains (in mM): 124 NaCl, 2.5 KCl, 1.25 NaH2PO4, 1 MgCl2, 26 NaHCO3, 11 glucose, 2.4 CaCl2, 0.05 caffeine, 300–310 mOsm, at pH 7.3–7.4. The recording ACSF is saturated with carbogen, maintained at 31-32°C, and perfused at 2 ml/min using a peristaltic pump. Caffeine, an adenosine A1 receptor antagonist, is used to reduce the effects of endogenous adenosine on observing CB1R function [37]. SCRAs are dissolved in ACSF containing 0.1% DMSO and 0.2-0.5% BSA, as SCRA lipophilicity can affect assay sensitivity [38]. Brain slices rest in perfused recording ACSF for 20 minutes before recording. A borosilicate recording electrode filled with recording ACSF is placed in the CA1 region of the hippocampus within the stratum radiatum, while a bipolar stimulating wire is placed in the CA3a region of the hippocampus. CA3 stimulation occurred at a frequency of 0.033 Hz, and were recorded using a MultiClamp 700b amplifier (10 kHz low-pass Bessel filter), digitized with a Digidata 1550b (20 kHz digitization), and visualized on pClamp software. Current amplitude is set at approximately 25-30% of max output, determined by generating an input/output curve. Baseline is recorded for 10 min before a 60-min drug perfusion.

2.6 Data Analysis

All data was processed and analyzed in GraphPad Prism 10 (San Diego, California). Data points were transformed to individual BRET ratio values and further normalized to the minimal and maximal responses by a reference full agonist CP55940 at 10 min as 0% and 100% respectively within each respective transducer. E_{max} and pEC_{50} parameters were obtained from the non-linear fit of normalized transformed data and multi-comparison data analyses at the 10 min time point were conducted. Based on the extrapolated curves, E_{max} and pEC_{50} are determined. E_{max} above 120% relative to the E_{max} of CP55,940 is interpreted as superagonist behavior. E_{max} on a non-plateaued curve and pEC_{50} less than 5 (i.e., 10 μM) are still reported in the tables. In those cases, E_{max} is reported as the efficacy at the highest concentration observed (10 μM). To evaluate whether SCRAs exhibited G protein subunit signaling bias, bias factors were calculated as reported previously [39]. This method yields bias factors similar to the operational model. Briefly, $\Delta\log(E_{max}/EC_{50})$ value for each transducer was calculated by subtracting the $\log(E_{max}/EC_{50})$ value of the agonist by that of the reference compound. $\Delta\Delta\log(E_{max}/EC_{50})$ is determined by subtraction of $\Delta\log(E_{max}/EC_{50})$ between two transducers. The comparison between the two transducers shows the bias direction of a certain ligand towards one of the two transducers. Throughout the experiments, a triplicate of at least four independent experiments was performed per each condition.

Statistical grouped analyses on E_{max} and pEC_{50} were conducted using one-way ANOVA with a post-hoc Dunnett test for multiple comparisons.

For extracellular recordings, the fEPSP slope was determined in Clampfit from a 1.5-2 ms range in the rise phase post-stimulation. Recordings were averaged in 2-min bins and inhibition was determined as the fEPSP slope percentage as compared to the baseline fEPSP slope. Max inhibition was determined by averaging the fEPSP slope of the last six min of the drug prefusion. Tau was obtained from the non-linear regression of the time course. Statistical significance of max inhibition and tau was determined using one-way ANOVA with a post-hoc Dunnett test for multiple comparisons.

3. Results

3.1 L-tert-leucinate head moiety leads to high efficacy in SCRA derivatives.

After recently investigating the drastic efficacy differences between l-valinate and l-*tert*-leucinate (*i.e.*, MMB- and MDMB-) head moieties of 5-fluoropenylindoles [31], we expanded our investigation on core and tail moieties in combination to the head moiety. Clinical studies have reported on the severe impact of indazole-based SCRA abuse, including death from overdose [3, 6, 40, 41]. Furthermore, original derivatives patented by Pfizer, as well as the drug responsible for the 2016 Brooklyn outbreak, carried a 4-fluorobenzyl tail moiety [6]. Therefore, we selected 5F-MMB-PICA (M-PC), 5F-MDMB-PICA (D-PC), 5F-MMB-PINACA (M-PN), 5F-MDMB-PINACA (D-PN), MMB-FUBICA (M-FC), MDMB-FUBICA (D-FC), MMB-FUBINACA (M-FN), MDMB-FUBINACA (D-FN) for our study panel to develop a SAR of these moieties for CB1R efficacy, thus investigating superagonism (Supp. Fig. 1).

We first measured the engagement of $G\alpha_{i1}$ and β-arrestin-2 to CB1R as they represent two major signaling modalities, using an “engagement” mode of BRET where the receptor and Gα-protein or β-arrestin are fused with luciferase and fluorescent proteins, respectively (Fig. 1A, 1C). Both M-PC and D-PC displayed superagonism (i.e., above 120%), although M-PC is ~20x less potent than D-PC in $G\alpha_{i1}$ engagement (Fig. 1A). We see a separation in both efficacy and potency for the 4-fluorobenzyl analogues M-FC and D-FC (Fig. 1B). Interestingly, the difference in efficacy between MMB- and MDMB-compounds is negligible amongst indazole SCRAs (*i.e.*, M-PN, D-PN, M-FN, D-FN), as all confer superagonism, although there is still a noticeable potency shift (~6-fold) for the MDMB- series (Fig. 1A-B, Table 1). Within the β-arrestin-2 engagement assay, seven of the eight SCRAs are more efficacious than the reference compound CP55,940, with only M-FC acting as a full agonist (Fig. 1C-D, Table 1). Although an insignificant difference for $G\alpha_{i1}$ engagement, the 5-fluoropentyl SCRAs were all approximately 20-75% greater in efficacy than their 4-fluorobenzyl analogues (Fig. 1C-D, Table 1).

3.2 SCRA superagonism is observed across activation of most $G\alpha_{i/o}$ subtypes.

Numerous studies have reported on SCRA-mediated CB1R activities without identifying the involvement of specific $G\alpha_{i/o}$ subtypes. Concurrently, there are limited findings on SCRA agonism amongst the six inhibitory G proteins ($G\alpha_{i1}$, $G\alpha_{i2}$, $G\alpha_{i3}$, $G\alpha_{oA}$, $G\alpha_{oB}$, $G\alpha_{z}$). Therefore, we studied the extent of SCRA superagonism across all six $G\alpha_{i/o}$ subtypes, as well as the contribution of key moieties of these SCRAs in the functional selectivity.

To investigate this, we use an "activation" mode of BRET to measure the G-protein heterotrimer dissociation via untagged CB1R (Fig. 2A, Table 2) [36, 42, 43]. In general, MDMB- compounds are more potent than MMB- compounds. Amongst indole SCRAs, there was a noticeable increase in both efficacy and potency for MDMB series compared to MMB series (Fig. 2B-G), but only an efficacy difference (>20%) for M-FC and D-FC in line with the $G\alpha_{i1}$ "engagement" assay results (Fig. 1A-B). M-FC showed the lowest efficacy and potency for $G\alpha_{i}$ subtypes; in the latter case, sharing the least potency with M-PC. For indazoles, MDMB- compounds are more potent than MMB- compounds, but there is no clear difference in efficacy in general. In $G\alpha_{oA}$, we found that D-PN was the single instance of an MDMB- indazole displaying noticeably greater efficacy (~50%) than its MMB- analogue (Fig. 2D, Table 2). Interestingly, a general high efficacy trend among all SCRAs tested (except for D-FC) was observed for $G\alpha_{i3}$ (>150%), $G\alpha_{oA}$ (>125%), and $G\alpha_{z}$ (>124%).

We further analyzed $G\alpha_{i/o}$ subtype activation by estimating each compound's functional selectivity by calculating bias factors. Here, we determined the $\Delta\log(E_{max}/EC_{50})$ of each SCRA to compare two different transducers then taking the difference between the Δ values of a particular SCRA and the reference agonist CP55,940, obtaining $\Delta\Delta\log(E_{max}/EC_{50})$ (Table 3). Here we found that none of the compounds had a ΔΔlog value outside the range of -1 to 1 (i.e., 10-fold separation between two $G\alpha_{i/o}$ subtypes relative to the reference CP55,940), thus suggesting the tested SCRAs are not significantly biased towards any specific pathway.

3.3 F170, F177, and H178 are key residues in SCRA activation, not exclusive to l-tert-leucinate.

After having established the consistent increase in efficacy and potency for l-*tert*-leucinate (*i.e.*, MDMB-) containing SCRAs, we investigated residues within the binding pocket essential for conferring superagonism. Recent research has found that extracellular transmembrane domain 2 (TM2) residues are implicated in CB1R activation as they rotate inwards in the presence of a full agonist [32, 33]. Indeed, we previously reported on the conformational stability of TM2 being associated with 5F-MDMB-PICA superagonism [31]. Here, we expanded our investigation by generating alanine substituted mutants along the TM2 residues in order to isolate the essential residues implicated in CB1R superagonism.

To that end, we generated alanine-substituted CB1R constructs at F170, S173, F174 F177, and H178, intracellular to extracellular on TM2, and assessed SCRA activity in these mutant constructs through $G\alpha_{i1}$ and β-arrestin-2 engagement BRET assays (Fig. 3-4). We selected the 5-fluoropentyl SCRAs (M-PC, D-PC, M-PN, D-PN) for this study, as these were the more efficacious compounds respective to their 4-fluorobenzyl analogs (Fig. 3A). By normalizing the E_{max} of CP55,940 for the wildtype CB1R as 100% efficacy, mutational effects on the SCRAs were studied.

In the $G\alpha_{i1}$ engagement assay, the F170A substitution blunted CP55,940 efficacy, and reduced the efficacy and potency of all the SCRAs tested, although M-PC had a lower efficacy than the other three (Fig. 3C, Table 4). The S173A substitution produced no significant change to the efficacy and potencies of the drugs tested (Fig. 3D, Table 4). Although F174A reduced the potency of the agonists, we observed a slight increase in the efficacy of these SCRAs relative to CP55,940 activity in wildtype CB1R (Fig. 3E, Table 4). The F177A mutation nearly blunted the efficacy of CP55,940, M-PC and M-PN, but only partially for D-PC and less so D-PN (Fig. 3F, Table 4). Similarly to F177A, the H178A mutation reduced the efficacy of CP55,940 and M-PC to low partial agonism, M-PN to high partial agonism, whereas D-PC and D-PN conferred high agonism (Fig. 3G, Table 4).

When comparing these results to β-arrestin-2 engagement, we find an overall rightward potency shift across the mutant constructs (Table 5). In F170A and S173A, we see similar efficacy reduction that we observed in $G\alpha_{i1}$ engagement (Fig. 4B-C). Although efficacy increased in CB1R F174A $G\alpha_{i1}$ engagement, SCRA efficacy was slightly reduced, relative to wildtype CB1R activity, in CB1R F174A β-arrestin-2 engagement. However, CP55,940 showed much higher efficacy reduction (71.5%) relative to wildtype, suggesting a differential residue-ligand interaction at F174 (Fig. 4D, Table 5). Interestingly, all drug response was flattened in CB1R F177A β-arrestin-2 engagement, where only l-*tert*-leucinate compounds had >30% efficacy (Fig. 4E, Table 5). In the H178A mutation results, we observed high efficacy in l-tert-leucinate compounds, and less than 35% efficacy in all other compounds (Fig. 4F, Table 5).

3.4 L-tert-leucinate SCRAs confer high efficacy agonism in glutamate release inhibition in the hippocampus.

To investigate the pharmacological profiles of SCRAs at a neurophysiological level, we evaluated the effects of l-*tert*-leucinate SCRAs through *ex vivo* brain slice electrophysiology. Specifically, CB1R-mediated suppression of neurotransmitter release was studied in the Schaffer collaterals of the hippocampus, as we have shown [31]. In the previous study, we reported that D-PC is significantly higher in efficacy compared to M-PC in inhibiting glutamate release in the hippocampus. Here, we evaluated the efficacy and kinetics of other l-*tert*-leucinate SCRAs on glutamate release.

We performed para-sagittal slicing of young adult mice brains to reveal the hippocampus and then perfused 1 μM, 300 nM, and 100 nM of SCRAs over the course of 60 minutes while recording field excitatory postsynaptic potentials (fEPSP) in the hippocampus (Fig. 5A, Supp. Fig. 4). l-valinate-containing M-PC was used as a reference SCRA against all l-*tert*-leucinate-containing (i.e., MDMB-) SCRAs. As expected, M-PC showed a low response, resulting in approximately 25% inhibition of the fEPSP slope. All four MDMB- compounds resulted in 40-55% inhibition, significantly greater than that of M-PC at 1 μM (Fig. 5B). When compared at lower concentrations, only 300 nM D-FC had a significantly lower inhibition than 1 μM (Fig. 6B). We also compared the kinetics of efficacy increase via CB1R over time with tau values of these compounds. We found that the tau for 1 μM D-PC and D-PN were under 10 minutes, whereas 1 μM D-FC and D-FN were ~10-20 minutes greater than that of M-PC, although these values were not determined to be significant (Fig. 5C). Although reaching significantly higher efficacy than M-PC, MDMB-SCRAs showed differential kinetics, specifically, slower response with 4-fluorobenzyl tail ones.

4. Discussion

Previous reports by others assessed a number of SCRAs used here as “high efficacy” agonists [28, 44, 45]. By using the BRET “engagement” mode, we can better address issues associated with signal amplification and receptor reserves, which can result in falsely high efficacy and potency activity in downstream functional assays [30, 46], whereas the engagement mode detect direct coupling between the receptor and transducer. Contrary to our previous results, M-PC displays superagonism for both Gαi1 and β-arrestin-2 engagement modes of BRET assays [26]. This likely resulted from adding 1 mg/mL BSA to the assay buffer as a carrier protein to these highly lipophilic compounds for their solubility and stability, as used in previous studies [21,22]. Nonetheless, D-PC shows remarkably higher potency compared to M-PC, consistent with our previous finding [31]. Indazoles, regardless of head or tail moiety within the structure, drastically increases SCRA efficacy and potency, the latter of which has been well reported for indazole SCRA derivatives [25, 26]. The superagonist activity of D-PC, D-PN, and D-FN, in both $G\alpha_{i/o}$ and β-arrestin engagement, likely contribute significantly to the severity of the adverse effects, as cannabis use, thus moderate efficacy of THC on CB1R, rarely causes the severe adverse effects and toxicities [10]. The increased efficacy in β-arrestin-2 engagement may be associated with increased tolerance found in SCRA use as β-arrestins mediate CB1R internalization [47, 48]. Indeed, SCRAs have been reported to induce rapid CB1R internalization through β-arrestin [26, 29]. These studies as well as our findings indicate that high efficacy in β-arrestin likely plays a role in adverse effects reported in human use.

Through G protein activation BRET assays, we determined that the panel of tested SCRAs displays superagonism across $G\alpha_{i/o}$ subtypes. This finding is crucial as most

previous reports have not focused on SCRA characterization of all $G\alpha_{i/o}$ subtypes as biased responses in different organs and cell-types can be implicated through diverse $G\alpha_{i/o}$ subtype expression. Indeed, the $G\alpha_{i1-3}$ are ubiquitously expressed throughout the body and are the dominant $G\alpha_{i/o}$ subtypes in the periphery, as the $G\alpha_{oA-B}$ and $G\alpha_z$ are the dominant proteins in the CNS. SCRA-induced superagonism across these subtypes may suggest a connection to the wide-range of adverse effects from SCRA use. We attempted to reveal any potential bias across head, core, and tail moieties by calculating ΔΔΔlog values from ΔΔlog of differing moieties (data not shown). However, we did not identify any significant bias beyond the -1 or 1 threshold, thus none of the moieties cause bias within $G\alpha_{i/o}$ subtypes. Other clinically reported SCRAs have also been found relatively balanced using similar *in vitro* assays [26-28]. Since there are a multitude of combinatorial diversity among different head, core and tail moieties for SCRAs, characterization of signaling bias remains to be explored and incomplete at present. Regardless, we have determined that across $G\alpha_{/o}$ subtypes, the panel of paired SCRA analogs at head, core and tail moieties display CB1R superagonism.

In the mutational study, we investigated the TM2 residues implicated in SCRA-mediated CB1R superagonism. Recent reports have indicated that H178 is implicated in the activation of the CB1R [32, 34]. We confirmed that to be the case as the alanine substitution drastically reduced the effect of CP55,940, M-PC, and M-PN in both engagement modes. This phenomenon implicates the ring structure and/or positive charge of histidine as essential in CB1R engagement to an agonist in general, beyond head moiety interaction in the aminoalkylindole agonists, warranting further investigation. We also found CP55,940 response was completely suppressed in F170A, F174A, and F177A, supporting results found recently in cAMP assays [34]. For the SCRAs, we expected that differences in the head moiety would lead to noticeable differences in activity in the more extracellular alanine substitutions in TM2, whereas the core moiety would be highlighted in the more intracellular substitutions. The alanine substitution at F170, the most intracellular residue tested, highlighted the difference in efficacy between MMB- and MDMB- compounds, but only for the indole compounds (M-PC, D-PC). Although M-PN has the less efficacious l-valinate head moiety, it remains as effective as D-PC and D-PN, suggesting an importance in the indazole stabilizing the active conformation. At only one residue down from the extracellular end H178 in TM2, F177A exhibited a clear separation in efficacy between MMB- and MDMB- compounds. Furthermore, this residue may be implicated in β-arrestin-2 bias, as even the l-*tert*-leucinate compounds showed significantly reduced efficacy, a distinct profile compared to that of F170 and H178. F174, in the middle of F170 and F177, seems necessary for CP55,940 activity, yet does not substantially impact SCRA efficacy and potency. To further characterize F174A, we tested the construct in $G\alpha_{oA}$ activation and found that the potency was reduced yet the efficacy had dramatically increased (Supp. Fig. 2D, Supp. Table 1). We found that the basal net BRET ratio for F174A was much higher than WT in $G\alpha_{oA}$

activation, indicating a lower constitutive receptor activity by the F174A mutation (Supp. Fig. 3C). However, the F174A construct remains capable of reaching levels of BRET on par with the wildtype at saturating agonist concentration, thus reaching the calculated high percentage of efficacy. We expected the head moiety of M-PC and D-PC to interact with S173 and, therefore, the S173A mutation to lower their efficacy [31]. Nonetheless, in our engagement assays, we did not observe a drastic efficacy decrease with S173A as in F170A and F177A. We did find an overall reduced efficacy in CB1R S173A $G\alpha_{oA}$ activation, yet SCRA efficacy and potency relative to CP55,940 efficacy and potency was similar to those found in wildtype CB1R $G\alpha_{oA}$ activation. (Supp. Fig. 2C, Supp. Table 1). Overall, S173 seems to have a smaller role in CB1R activity compared to the other TM2 residues tested. Further investigation of interacting residues beyond these TM2 residues will provide more insight into SCRA superagonism and key interactions with SCRA core and tail moieties as well.

In the field recording of hippocampal slices, we confirmed that l-*tert*-leucinate SCRAs confer a high degree of efficacy at a neurophysological level. Interestingly, M-PC confers a distinctly lower level of efficacy to D-PC in electrophysiology that we do not see in our BRET studies. That is, despite the addition of BSA, field recordings did not differ much from our previous results. However, when compared to BRET results with BSA addition, the significant efficacy difference between M-PC and D-PC is gone. Although all MDMB-compounds had much greater levels of inhibition, the tail moiety seemed to play some role in the kinetics of these drugs, given the higher tau for 4-fluorobenzyl (i.e., D-FC and D-FN) than 5-fluoropentyl compounds (i.e., M-PC, D-PC, and D-PN). This difference may be due to the higher lipophilicity of the benzyl ring in the tail moiety (e.g., cLogP values: M-PC – 3.9, D-PC – 4.3, D-FC – 4.7, D-PN – 4.2, D-FN – 4.6), potentially leading to reduced solubility and receptor access. Indeed, kinetic differences were not observed among MDMB- compounds in *in vitro* BRET assays as there is no tissue penetration involved for the receptor activity. Within the 4-fluorobenzyl SCRAs, we do see that the indole (D-FC) is less potent than D-FN, given the difference in efficacy at 300 nM. As such our electrophysiological recordings can be a viable method to distinguish ligand accessibility to native CB1Rs and evaluate their efficacy at neurons.

5. Conclusion

The iterative design of SCRAs in their modular components has led to an explosive number of substances, many manifested toxicities. In this study, we attempted to understand the involvement of TM2 in a SAR for SCRA-induced CB1R superagonism. Using structural pairwise comparison within head, core, and tail moieties, we detailed superagonism conferred by the l-*tert*-leucinate head moiety. We found that SCRAs, depending on their key moieties, can elicit superagonism through multiple $G\alpha_{i/o}$ subtypes and β-arrestin, and that F170, F177, and H178 in TM2 are implicated in conferring such drug action. This pairwise comparison approach within ligand structure in conjunction with

extensive transducer analysis may be useful for revealing specific activation profiles in the future SAR studies for novel SCRAs.

CRediT authorship contribution statement

Christopher Lucaj: Conceptualization, Data curation, Formal analysis, Investigation, Methodology, Validation, Visualization, Writing – original draft, Writing – review & editing. **Soo Jung Oh:** Investigation, Methodology **Charlotte Pitha:** Investigation, Methodology **Jordan Davis:** Investigation, Methodology **Hideaki Yano:** Conceptualization, Data curation, Formal analysis, Project administration, Resources, Funding acquisition, Supervision, Writing – original draft, Writing – review & editing

Acknowledgements and Funding

The work is supported by the Brain & Behavior Research Foundation Young Investigator Grant (H.Y.) and by the National Institute on Drug Abuse (T32DA055553 to C.L.) We would like to thank Dr. Carl Lupica and Dr. Alexander Hoffman for technical advice and discussion on brain slice electrophysiology.

References

1. Huffman JW, Dai D., Martin B.R., Compton D.R.: **Design, synthesis and pharmacology of cannabimimetic indoles**. *Bioorganic & Medicinal Chemistry Letters* 1994, **4**(4):563-566.
2. Wiley JL, Compton DR, Dai D, Lainton JA, Phillips M, Huffman JW, Martin BR: **Structure-activity relationships of indole- and pyrrole-derived cannabinoids**. *J Pharmacol Exp Ther* 1998, **285**(3):995-1004.
3. Schwartz MD, Trecki J, Edison LA, Steck AR, Arnold JK, Gerona RR: **A Common Source Outbreak of Severe Delirium Associated with Exposure to the Novel Synthetic Cannabinoid ADB-PINACA**. *J Emerg Med* 2015, **48**(5):573-580.
4. Zapata F, Matey JM, Montalvo G, García-Ruiz C: **Chemical classification of new psychoactive substances (NPS)**. *Microchemical Journal* 2021, **163**:105877.
5. UNODC: **World Drug Report 2024**. In.; 2024.
6. Adams AJ, Banister SD, Irizarry L, Trecki J, Schwartz M, Gerona R: **"Zombie" Outbreak Caused by the Synthetic Cannabinoid AMB-FUBINACA in New York**. *N Engl J Med* 2017, **376**(3):235-242.
7. Craft S, Ferris JA, Barratt MJ, Maier LJ, Lynskey MT, Winstock AR, Freeman TP: **Clinical withdrawal symptom profile of synthetic cannabinoid receptor agonists and comparison of effects with high potency cannabis**. *Psychopharmacology* 2022, **239**(5):1349-1357.
8. Prete MM, Feitosa GTB, Ribeiro MAT, Fidalgo TM, Sanchez ZM: **Adverse clinical effects associated with the use of synthetic cannabinoids: A systematic review**. *Drug and Alcohol Dependence* 2025, **272**:112698.
9. Zaurova M, Hoffman RS, Vlahov D, Manini AF: **Clinical Effects of Synthetic Cannabinoid Receptor Agonists Compared with Marijuana in Emergency Department Patients with Acute Drug Overdose**. *J Med Toxicol* 2016, **12**(4):335-340.
10. Ford BM, Tai S, Fantegrossi WE, Prather PL: **Synthetic Pot: Not Your Grandfather's Marijuana**. *Trends Pharmacol Sci* 2017, **38**(3):257-276.
11. Tokarczyk B, Jurczyk A, Krupińska J, Adamowicz P: **Fatal intoxication with new synthetic cannabinoids 5F-MDMB-PICA and 4F-MDMB-BINACA—parent compounds and metabolite identification in blood, urine and cerebrospinal fluid**. *Forensic Science, Medicine and Pathology* 2022, **18**(4):393-402.
12. Simon G, Kuzma M, Mayer M, Petrus K, Tóth D: **Fatal Overdose with the Cannabinoid Receptor Agonists MDMB-4en-PINACA and 4F-ABUTINACA: A Case Report and Review of the Literature**. *Toxics* 2023, **11**(8):673.
13. Marsicano G, Lutz B: **Expression of the cannabinoid receptor CB1 in distinct neuronal subpopulations in the adult mouse forebrain**. *Eur J Neurosci* 1999, **11**(12):4213-4225.
14. Kano M, Ohno-Shosaku T, Maejima T: **Retrograde signaling at central synapses via endogenous cannabinoids**. *Mol Psychiatry* 2002, **7**(3):234-235.
15. Piomelli D: **The molecular logic of endocannabinoid signalling**. *Nat Rev Neurosci* 2003, **4**(11):873-884.

16. Ohno-Shosaku T, Tsubokawa H, Mizushima I, Yoneda N, Zimmer A, Kano M: **Presynaptic cannabinoid sensitivity is a major determinant of depolarization-induced retrograde suppression at hippocampal synapses**. *J Neurosci* 2002, **22**(10):3864-3872.
17. Ravinet Trillou C, Delgorge C, Menet C, Arnone M, Soubrié P: **CB1 cannabinoid receptor knockout in mice leads to leanness, resistance to diet-induced obesity and enhanced leptin sensitivity**. *Int J Obes Relat Metab Disord* 2004, **28**(4):640-648.
18. Mendizábal VE, Adler-Graschinsky E: **Cannabinoids as therapeutic agents in cardiovascular disease: a tale of passions and illusions**. *Br J Pharmacol* 2007, **151**(4):427-440.
19. Malinowska B, Baranowska-Kuczko M, Schlicker E: **Triphasic blood pressure responses to cannabinoids: do we understand the mechanism?** *Br J Pharmacol* 2012, **165**(7):2073-2088.
20. Jiang M, Bajpayee NS: **Molecular mechanisms of go signaling**. *Neurosignals* 2009, **17**(1):23-41.
21. Foerster K, Groner F, Matthes J, Koch WJ, Birnbaumer L, Herzig S: **Cardioprotection specific for the G protein Gi2 in chronic adrenergic signaling through beta 2-adrenoceptors**. *Proc Natl Acad Sci U S A* 2003, **100**(24):14475-14480.
22. Cha HL, Choi JM, Oh HH, Bashyal N, Kim SS, Birnbaumer L, Suh-Kim H: **Deletion of the α subunit of the heterotrimeric Go protein impairs cerebellar cortical development in mice**. *Mol Brain* 2019, **12**(1):57.
23. Hultman R, Kumari U, Michel N, Casey PJ: **Gαz regulates BDNF-induction of axon growth in cortical neurons**. *Mol Cell Neurosci* 2014, **58**:53-61.
24. Banister SD, Longworth M, Kevin R, Sachdev S, Santiago M, Stuart J, Mack JB, Glass M, McGregor IS, Connor M *et al*: **Pharmacology of Valinate and tert-Leucinate Synthetic Cannabinoids 5F-AMBICA, 5F-AMB, 5F-ADB, AMB-FUBINACA, MDMB-FUBINACA, MDMB-CHMICA, and Their Analogues**. *ACS Chem Neurosci* 2016, **7**(9):1241-1254.
25. Banister SD, Moir M, Stuart J, Kevin RC, Wood KE, Longworth M, Wilkinson SM, Beinat C, Buchanan AS, Glass M *et al*: **Pharmacology of Indole and Indazole Synthetic Cannabinoid Designer Drugs AB-FUBINACA, ADB-FUBINACA, AB-PINACA, ADB-PINACA, 5F-AB-PINACA, 5F-ADB-PINACA, ADBICA, and 5F-ADBICA**. *ACS Chem Neurosci* 2015, **6**(9):1546-1559.
26. Finlay DB, Manning JJ, Ibsen MS, Macdonald CE, Patel M, Javitch JA, Banister SD, Glass M: **Do Toxic Synthetic Cannabinoid Receptor Agonists Have Signature in Vitro Activity Profiles? A Case Study of AMB-FUBINACA**. *ACS Chem Neurosci* 2019, **10**(10):4350-4360.
27. Patel M, Manning JJ, Finlay DB, Javitch JA, Banister SD, Grimsey NL, Glass M: **Signalling profiles of a structurally diverse panel of synthetic cannabinoid receptor agonists**. *Biochem Pharmacol* 2020, **175**:113871.
28. Ryalls B, Patel M, Sparkes E, Banister SD, Finlay DB, Glass M: **Investigating selectivity and bias for G protein subtypes and β-arrestins by synthetic cannabinoid receptor agonists at the cannabinoid CB1 receptor**. *Biochemical Pharmacology* 2024, **222**:116052.

29. Zagzoog A, Brandt AL, Black T, Kim ED, Burkart R, Patel M, Jin Z, Nikolaeva M, Laprairie RB: **Assessment of select synthetic cannabinoid receptor agonist bias and selectivity between the type 1 and type 2 cannabinoid receptor**. *Sci Rep* 2021, **11**(1):10611.
30. Schrage R, De Min A, Hochheiser K, Kostenis E, Mohr K: **Superagonism at G protein-coupled receptors and beyond**. *Br J Pharmacol* 2016, **173**(20):3018-3027.
31. Yano H, Chitsazi R, Lucaj C, Tran P, Hoffman AF, Baumann MH, Lupica CR, Shi L: **Subtle Structural Modification of a Synthetic Cannabinoid Receptor Agonist Drastically Increases its Efficacy at the CB1 Receptor**. *ACS Chemical Neuroscience* 2023, **14**(21):3928-3940.
32. Krishna Kumar K, Robertson MJ, Thadhani E, Wang H, Suomivuori CM, Powers AS, Ji L, Nikas SP, Dror RO, Inoue A *et al*: **Structural basis for activation of CB1 by an endocannabinoid analog**. *Nat Commun* 2023, **14**(1):2672.
33. Krishna Kumar K, Shalev-Benami M, Robertson MJ, Hu H, Banister SD, Hollingsworth SA, Latorraca NR, Kato HE, Hilger D, Maeda S *et al*: **Structure of a Signaling Cannabinoid Receptor 1-G Protein Complex**. *Cell* 2019, **176**(3):448-458.e412.
34. Brust CA, Swanson MA, Tsoutsouvas CI, Dimova ST, Dang VQ, Stahl EL, Ho J-H, Nikas SP, Makriyannis A, Bohn LM: **Comparison of Agonist Activity between CB1 and CB2 Receptors with Orthosteric Site Mutations**. *Receptors* 2024, **3**(3):380-396.
35. Semeano A, Garland R, Bonifazi A, Lee KH, Famiglietti J, Zhang W, Jo YJ, Battiti FO, Shi L, Newman AH *et al*: **Linkers in Bitopic Agonists Shape Bias Profile among Transducers for the Dopamine D2 and D3 Receptors**. *ACS Pharmacology & Translational Science* 2024, **7**(8):2333-2349.
36. Sánchez-Soto M, Bonifazi A, Cai NS, Ellenberger MP, Newman AH, Ferré S, Yano H: **Evidence for Noncanonical Neurotransmitter Activation: Norepinephrine as a Dopamine D₂-Like Receptor Agonist**. *Molecular Pharmacology* 2016, **89**(4):457-466.
37. Hoffman AF, Laaris N, Kawamura M, Masino SA, Lupica CR: **Control of cannabinoid CB1 receptor function on glutamate axon terminals by endogenous adenosine acting at A1 receptors**. *J Neurosci* 2010, **30**(2):545-555.
38. Báldi R, Ghosh D, Grueter BA, Patel S: **Electrophysiological Measurement of Cannabinoid-Mediated Synaptic Modulation in Acute Mouse Brain Slices**. *Current Protocols in Neuroscience* 2016, **75**(1):6.29.21-26.29.19.
39. Bonifazi A, Yano H, Guerrero AM, Kumar V, Hoffman AF, Lupica CR, Shi L, Newman AH: **Novel and Potent Dopamine D(2) Receptor Go-Protein Biased Agonists**. *ACS Pharmacol Transl Sci* 2019, **2**(1):52-65.
40. Usui K, Fujita Y, Kamijo Y, Kokaji T, Funayama M: **Identification of 5-fluoro ADB in human whole blood in four death cases**. *Journal of analytical toxicology* 2018, **42**(2):e21-e25.
41. Boland DM, Reidy LJ, Seither JM, Radtke JM, Lew EO: **Forty-three fatalities involving the synthetic cannabinoid, 5-fluoro-ADB: Forensic pathology and toxicology implications**. *Journal of forensic sciences* 2020, **65**(1):170-182.

42. Galés C, Van Durm JJJ, Schaak S, Pontier S, Percherancier Y, Audet M, Paris H, Bouvier M: **Probing the activation-promoted structural rearrangements in preassembled receptor–G protein complexes**. *Nature Structural & Molecular Biology* 2006, **13**(9):778-786.
43. Yano H, Sánchez-Soto M, Ferré S: **Bioluminescence Resonance Energy Transfer Assay to Characterize Gi-Like G Protein Subtype-Dependent Functional Selectivity**. *Curr Protoc Neurosci* 2017, **81**:5.33.31-35.33.13.
44. Cabanlong CV, Russell LN, Fantegrossi WE, Prather PL: **Metabolites of Synthetic Cannabinoid 5F-MDMB-PINACA Retain Affinity, Act as High Efficacy Agonists and Exhibit Atypical Pharmacodynamic Properties at CB1 Receptors**. *Toxicol Sci* 2022, **187**(1):175-185.
45. Banister SD, Connor M: **The Chemistry and Pharmacology of Synthetic Cannabinoid Receptor Agonists as New Psychoactive Substances: Origins**. *Handb Exp Pharmacol* 2018, **252**:165-190.
46. Schrage R, Seemann WK, Klöckner J, Dallanoce C, Racké K, Kostenis E, De Amici M, Holzgrabe U, Mohr K: **Agonists with supraphysiological efficacy at the muscarinic M2 ACh receptor**. *Br J Pharmacol* 2013, **169**(2):357-370.
47. Daigle TL, Kwok ML, Mackie K: **Regulation of CB1 cannabinoid receptor internalization by a promiscuous phosphorylation-dependent mechanism**. *J Neurochem* 2008, **106**(1):70-82.
48. Jin W, Brown S, Roche JP, Hsieh C, Celver JP, Kovoor A, Chavkin C, Mackie K: **Distinct domains of the CB1 cannabinoid receptor mediate desensitization and internalization**. *J Neurosci* 1999, **19**(10):3773-3780.

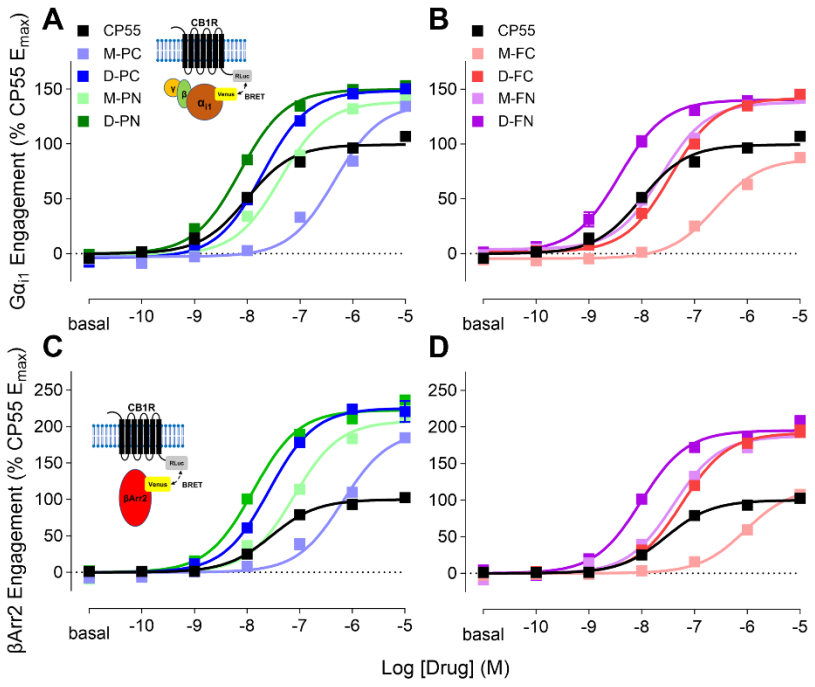

Figure 1: SCRA-induced $G\alpha_{i1}$ and β-arrestin-2 engagement to CB1R. Drug-induced BRET between CB1R-RLuc and $G\alpha_{i1}$-Venus (A,B) or βArr2-Venus (C,D) are shown. Concentration-response curves of SCRA-induced BRET are plotted as a percentage of CP55 E_{max} (A,B, $G\alpha_{i1}$; C,D, βArr2) and organized by tail moiety (A,C 5-fluoropentyl; B,D 4-fluorobenzyl). Data are presented as means ± SEM of n=4 experiments.

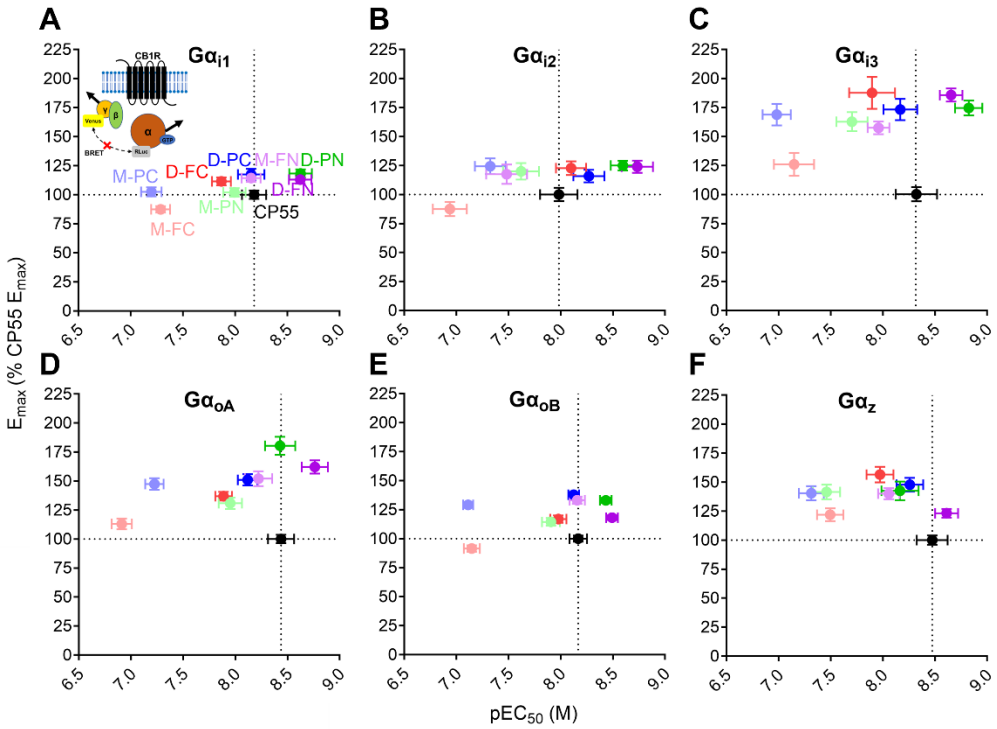

Figure 2: SCRA-activated $G\alpha_{i/o}$ subtype protein dissociation BRET assay. Cartoon illustrating BRET interaction between CB1R and Gα-RLuc and $G\gamma_2$-Venus with untagged CB1R (A, insert). SCRA-induced BRET efficacy, as a percentage of CP55 E_{max}, and pEC50 were plotted for $G\alpha_{i/o}$ subtype transducers: $G\alpha_{i1}$ (A), $G\alpha_{i2}$ (B), $G\alpha_{i3}$ (C), $G\alpha_{oA}$ (D), $G\alpha_{oB}$ (E), and $G\alpha_z$ (F). Data presented as means ± SEM of n≥4 experiments. The full concentration-response curves can be found in Supplementary Figure 2.

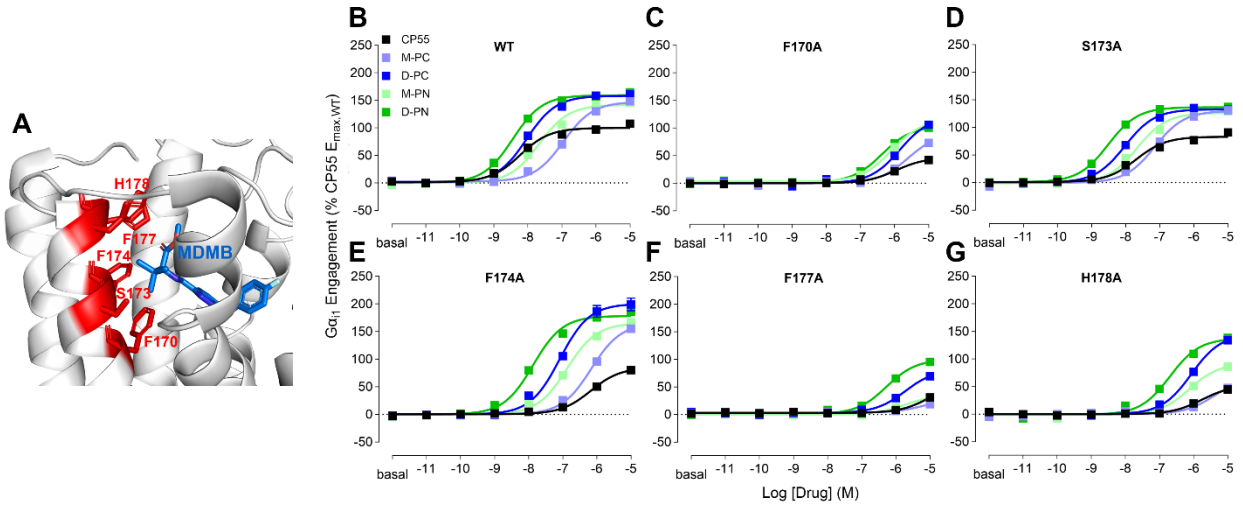

Figure 3: CB1R-TM2 mutational analysis of G-protein engagement. A close-up view of TM2-MDMB-FUBINACA (PDB:6N4B) with residues (red) within 4 Å of the MDMB-head moiety (blue) using PyMOL 3.0 (Schrödinger) for visualization (A). Through BRET $G\alpha_{i1}$ Engagement mode, M-PC, D-PC, M-PN, and D-PN are compared to CP55 in the presence of CB1R with the following TM2 mutations: Wildtype (B), F170A (C), S173A (D), F174A (E), F177A (F), H178A (G). Concentration-response curves of SCRA-induced BRET plotted as a percentage of CP55 $E_{max,WT}$. Data presented as means ± SEM of n=4 experiments.

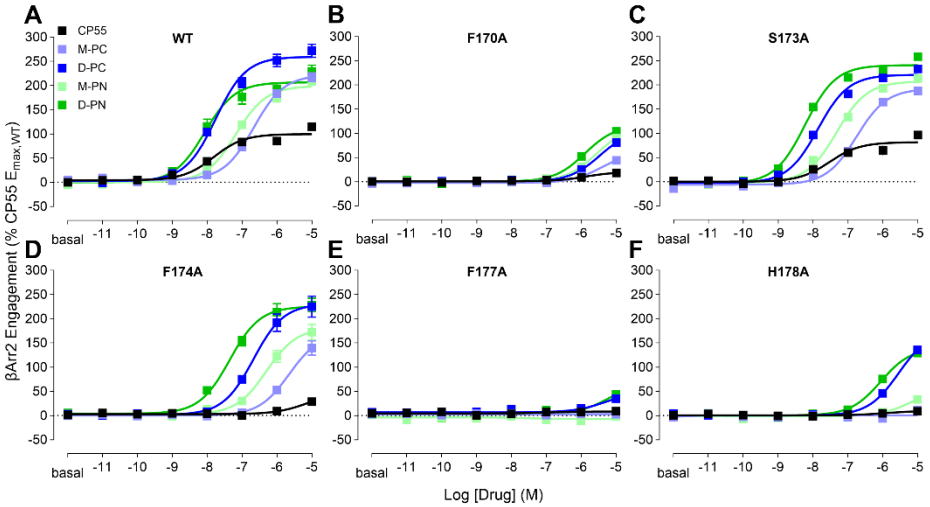

Figure 4: CB1R-TM2 mutational analysis of β-arrestin-2 engagement. Through BRET βArr2 Engagement mode, M-PC, D-PC, M-PN, and D-PN are compared to CP55 in the presence of CB1R with the following TM2 mutations: Wildtype (A), F170A (B), S173A (C), F174A (D), F177A (E), H178A (F). Concentration-response curves of SCRA-induced BRET plotted as a percentage of CP55 $E_{max,WT}$. Data presented as means ± SEM of n=4 experiments.

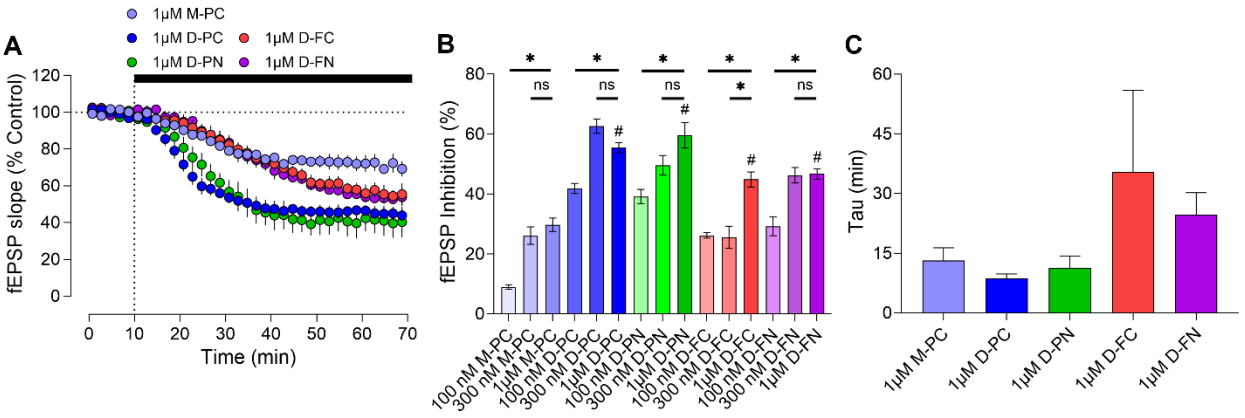

Figure 5: Extracellular field recordings in the CA1 hippocampus after perfusion of L-*tert*-leucinate SCRAs. Field extracellular postsynaptic potentials (fEPSPs) were recorded every 30 seconds in the CA1 hippocampus during SCRA perfusion. After 10 minutes of baseline, SCRAs were perfused for 60 minutes (A). Maximum inhibition was calculated from the average of the last six minutes of 1 μM, 300 nM, 100 nM SCRA perfusion (B). The time decay constant tau was calculated from the fitted curve of the timecourse recording (C). (N≥4 mice; n≥4 recordings; means ± SEM; $p<0.05$ compared to respective 1 μM SCRA = *, $p<0.05$ compared 1 μM M-PC = #.)

Table 1: Pharmacological comparison of SCRAs in CB1R-transducer engagement BRET

	$G\alpha_{i1}$		βArr2		Bias Factor	
	E_{max} (% CP55)	pEC_{50} (M)	E_{max} (% CP55)	pEC_{50} (M)	ΔΔlog	$G\alpha_{i1}$ - βArr2
CP55	100.0 ± 1.75	8.01 ± 0.05	100.0 ± 1.59	7.54 ± 0.10		
M-PC	136.5 ± 3.97*	6.34 ± 0.06*	193.7 ± 5.71*	6.19 ± 0.05*	**M-PC - CP55**	-0.47
D-PC	148.6 ± 1.71*	7.71 ± 0.03*	225.1 ± 4.17*	7.58 ± 0.06	**D-PC - CP55**	-0.52
M-PN	138.5 ± 2.79*	7.37 ± 0.06*	207.6 ± 3.92*	7.11 ± 0.06*	**M-PN - CP55**	-0.39
D-PN	149.6 ± 2.07*	8.14 ± 0.04	222.5 ± 2.74*	7.89 ± 0.09*	**D-PN - CP55**	-0.40
M-FC	86.5 ± 3.42*	6.61 ± 0.09*	117.3 ± 4.60*	6.04 ± 0.13*	**M-FC - CP55**	-0.03
D-FC	131.0 ± 2.40*	7.44 ± 0.06*	191.9 ± 3.31*	7.23 ± 0.05*	**D-FC - CP55**	-0.40
M-FN	137.8 ± 2.45*	7.63 ± 0.05*	187.5 ± 2.98*	7.40 ± 0.08	**M-FN - CP55**	-0.37
D-FN	140.2 ± 2.50*	8.42 ± 0.06*	195.2 ± 3.29*	8.02 ± 0.08*	**D-FN - CP55**	-0.21

Data analyzed by one-way ANOVA followed by post-hoc Dunnett test. Data presented as means ± SEM. Significance of * represents p<0.05 compared to CP55 E_{max} and pEC_{50} values for respective transducer.

Table 2: Pharmacological comparison of SCRAs in G protein dissociation BRET

	$G\alpha_{i1}$		$G\alpha_{i2}$		$G\alpha_{i3}$		$G\alpha_{oA}$		$G\alpha_{oB}$		$G\alpha_{z}$	
	E_{max} (% CP55)	pEC_{50} (M)	E_{max} (% CP55)	pEC_{50} (M)	E_{max} (% CP55)	pEC_{50} (M)	E_{max} (% CP55)	pEC_{50} (M)	E_{max} (% CP55)	pEC_{50} (M)	E_{max} (% CP55)	pEC_{50} (M)
CP55	100.0 ± 3.66	8.18 ± 0.12	100.0 ± 5.87	7.98 ± 0.18	100.3 ± 6.19	8.32 ± 0.20	100.0 ± 3.63	8.44 ± 0.12	100.0 ± 2.68	8.17 ± 0.084	100.0 ± 4.11	8.47 ± 0.15
M-PC	102.6 ± 3.97	7.20 ± 0.10*	124.4 ± 6.77	7.32 ± 0.15*	168.9 ± 9.32*	6.98 ± 0.13*	147.4 ± 5.06*	7.22 ± 0.09*	129.2 ± 2.51*	7.11 ± 0.05*	140.4 ± 6.16*	7.32 ± 0.12*
D-PC	117.6 ± 4.83*	8.15 ± 0.13	115.9 ± 5.36	8.27 ± 0.15	173.3 ± 9.10*	8.17 ± 0.16	151.0 ± 4.89*	8.12 ± 0.09	137.9 ± 2.33*	8.12 ± 0.05	147.8 ± 5.95*	8.26 ± 0.13
M-PN	102.1 ± 3.68	7.99 ± 0.11	120.1 ± 7.12	7.62 ± 0.17	162.8 ± 8.30*	7.70 ± 0.15*	130.9 ± 4.88*	7.95 ± 0.11*	114.6 ± 3.36*	7.91 ± 0.09	141.5 ± 6.30*	7.46 ± 0.13*
D-PN	118.3 ± 3.63*	8.63 ± 0.11*	125.1 ± 4.20*	8.60 ± 0.12	174.7 ± 6.40*	8.82 ± 0.13	180.4 ± 7.84*	8.43 ± 0.14	133.1 ± 2.20*	8.43 ± 0.06	142.5 ± 8.11*	8.17 ± 0.18
M-FC	87.5 ± 2.90	7.29 ± 0.09*	87.5 ± 6.17	6.94 ± 0.16*	126.0 ± 9.93	7.15 ± 0.19*	113.0 ± 4.64	6.91 ± 0.10*	91.6 ± 2.81	7.15 ± 0.08*	121.9 ± 5.50	7.50 ± 0.13*
D-FC	111.6 ± 3.45	7.87 ± 0.09	122.8 ± 5.91	8.10 ± 0.14	187.7 ± 13.79*	7.90 ± 0.22*	136.9 ± 3.73*	7.89 ± 0.08*	116.9 ± 3.12*	7.98 ± 0.08	156.5 ± 6.81*	7.97 ± 0.13
M-FN	114.4 ± 3.33	8.15 ± 0.09	117.5 ± 8.48	7.48 ± 0.20	157.5 ± 5.57*	7.96 ± 0.10*	152.1 ± 6.38*	8.22 ± 0.13	133.2 ± 3.13*	8.16 ± 0.07	140.0 ± 4.75*	8.06 ± 0.10
D-FN	113.1 ± 3.47	8.62 ± 0.11*	124.0 ± 5.29	8.73 ± 0.15	185.8 ± 5.68*	8.66 ± 0.11	162.2 ± 5.79*	8.76 ± 0.13	118.2 ± 1.95*	8.49 ± 0.07	123.3 ± 3.81*	8.61 ± 0.11

Data analyzed by one-way ANOVA followed by post-hoc Dunnett test. Data presented as means ± SEM. Significance of * represents p<0.05.

Table 3: SCRA-mediated activation bias of $G\alpha_{i/o}$ subtypes

ΔΔlog	$G\alpha_{i1}$ - $G\alpha_{i2}$	$G\alpha_{i1}$ - $G\alpha_{i3}$	$G\alpha_{i1}$ - $G\alpha_{oA}$	$G\alpha_{i1}$ - $G\alpha_{oB}$	$G\alpha_{i1}$ - $G\alpha_{z}$	$G\alpha_{i2}$ - $G\alpha_{i3}$	$G\alpha_{i2}$ - $G\alpha_{oA}$	$G\alpha_{i2}$ - $G\alpha_{oB}$	$G\alpha_{i2}$ - $G\alpha_{z}$	$G\alpha_{i3}$ - $G\alpha_{oA}$	$G\alpha_{i3}$ - $G\alpha_{oB}$	$G\alpha_{i3}$ - $G\alpha_{z}$	$G\alpha_{oA}$ - $G\alpha_{oB}$	$G\alpha_{oA}$ - $G\alpha_{z}$	$G\alpha_{oB}$ - $G\alpha_{z}$
M-PC - CP55	-0.41	0.14	0.07	-0.03	0.04	0.55	0.48	0.38	0.45	-0.07	-0.17	-0.10	-0.10	-0.03	0.07
D-PC - CP55	-0.31	-0.04	0.18	-0.05	0.09	0.27	0.49	0.26	0.40	0.22	-0.01	0.13	-0.24	-0.10	0.14
M-PN - CP55	0.10	0.23	0.19	0.02	0.68	0.13	0.09	-0.08	0.58	-0.04	-0.20	0.45	-0.17	0.49	0.66
D-PN - CP55	-0.19	-0.23	0.27	0.13	0.67	-0.03	0.46	0.32	0.87	0.50	0.35	0.90	-0.14	0.40	0.54
M-FC - CP55	0.15	0.12	0.52	0.11	-0.06	-0.03	0.37	-0.04	-0.21	0.40	-0.01	-0.18	-0.41	-0.58	-0.17
D-FC - CP55	-0.47	-0.11	0.15	-0.14	0.04	0.36	0.62	0.33	0.51	0.26	-0.03	0.15	-0.29	-0.11	0.18
M-FN - CP55	0.46	0.20	0.06	-0.09	0.30	-0.26	-0.40	-0.55	-0.16	-0.13	-0.28	0.10	-0.15	0.24	0.39
D-FN - CP55	-0.35	-0.11	-0.04	0.10	0.27	0.24	0.31	0.45	0.62	0.07	0.20	0.37	0.14	0.31	0.17

Table 4: CB1R-TM2 Mutational Analysis with SCRA Head Moiety ($G\alpha_{i1}$ Engagement)

	WT		F170A		S173A		F174A		F177A		H178A	
	E_{max} (% CP55,WT)	pEC_{50} (M)	E_{max} (% CP55,WT)	pEC_{50} (M)	E_{max} (% CP55,WT)	pEC_{50} (M)	E_{max} (% CP55,WT)	pEC_{50} (M)	E_{max} (% CP55,WT)	pEC_{50} (M)	E_{max} (% CP55,WT)	pEC_{50} (M)
CP55	100.0 ± 1.31	8.23 ± 0.04	42.2 ± 3.78	N.D.	83.1 ± 1.62	7.70 ± 0.06	85.0 ± 3.41	6.18 ± 0.08*	31.0 ± 2.17	N.D.	44.7 ± 3.33	N.D.
M-PC	147.4 ± 2.06*	6.96 ± 0.03*	72.9 ± 3.02	N.D.	130.1 ± 1.96*	7.15 ± 0.04*	164.9 ± 4.15*	6.17 ± 0.05*	18.8 ± 1.27	N.D.	47.5 ± 2.74	N.D.
D-PC	158.3 ± 1.78*	8.04 ± 0.03	121.3 ± 4.59*	5.84 ± 0.06*	132.8 ± 1.15*	8.02 ± 0.03	200.4 ± 4.99*	7.09 ± 0.06*	69.5 ± 2.89	N.D.	145.3 ± 3.83*	6.06 ± 0.05*
M-PN	141.8 ± 1.85*	7.67 ± 0.04	114.7 ± 3.85	6.01 ± 0.06*	126.3 ± 1.50*	7.67 ± 0.03	165.3 ± 2.43*	6.88 ± 0.03*	29.9 ± 3.21	N.D.	92.5 ± 3.93	6.12 ± 0.08*
D-PN	159.4 ± 1.91*	8.45 ± 0.04	104.1 ± 3.34	6.37 ± 0.07*	136.6 ± 1.14*	8.52 ± 0.03	178.3 ± 1.73*	7.87 ± 0.03	100.3 ± 2.89	6.27 ± 0.06*	137.6 ± 2.75*	6.70 ± 0.05*

Data analyzed by one-way ANOVA followed by post-hoc Dunnett test. Data presented as means ± SEM. Significance of * represents p<0.05 compared to CP55 E_{max}, pEC_{50} of the wildtype construct. For concentration-response curves with a low potency shift and/or low E_{max} the pEC_{50} was not determined (N.D.) and the E_{max} shown is the effect at the maximum concentration tested (10 μM).

Table 5: CB1R-TM2 Mutational Analysis with SCRA Head Moiety (βArr2 Engagement)

	WT		F170A		S173A		F174A		F177A		H178A	
	E_{max} (% CP55,WT)	pEC_{50} (M)	E_{max} (% CP55,WT)	pEC_{50} (M)	E_{max} (% CP55,WT)	pEC_{50} (M)	E_{max} (% CP55,WT)	pEC_{50} (M)	E_{max} (% CP55,WT)	pEC_{50} (M)	E_{max} (% CP55,WT)	pEC_{50} (M)
CP55	100.0 ± 2.76*	7.82 ± 0.08	18.3 ± 1.94	N.D.	81.6 ± 3.90	7.53 ± 0.14	28.5 ± 3.51	N.D.	8.82 ± 1.84	N.D.	8.61 ± 4.39	N.D.
M-PC	221.9 ± 4.47*	6.66 ± 0.05	43.9 ± 6.77	N.D.	192.4 ± 7.79*	6.76 ± 0.09	170.7 ± 12.36*	5.65 ± 0.11	2.71 ± 2.56	N.D.	11.3 ± 2.10	N.D.
D-PC	259.3 ± 5.39*	7.76 ± 0.06	80.7 ± 7.77	N.D.	221.1 ± 7.06*	7.86 ± 0.09	230.7 ± 9.67*	6.68 ± 0.10	34.9 ± 2.66	N.D.	135.6 ± 6.39	N.D.
M-PN	199.0 ± 4.54*	7.17 ± 0.06	90.4 ± 6.60	N.D.	207.3 ± 8.10*	7.32 ± 0.10	181.2 ± 8.75*	6.30 ± 0.10	-2.0 ± 3.44	N.D.	33.4 ± 3.45	N.D.
D-PN	206.6 ± 6.56*	8.07 ± 0.10	117.1 ± 6.06	5.9 ± 0.09	240.9 ± 8.86*	8.23 ± 0.11	225.3 ± 6.71*	7.356 ± 0.08	43.5 ± 5.29	N.D.	141.0 ± 4.79	6.05 ± 0.06

Data analyzed by one-way ANOVA followed by post-hoc Dunnett test. Data presented as means ± SEM. Significance of * represents $p<0.05$ compared to CP55 E_{max}, pEC_{50} of the wildtype construct. For concentration-response curves with a low potency shift and/or low E_{max} the pEC_{50} was not determined (N.D.) and the E_{max} shown is the effect at the maximum concentration tested (10 μM).

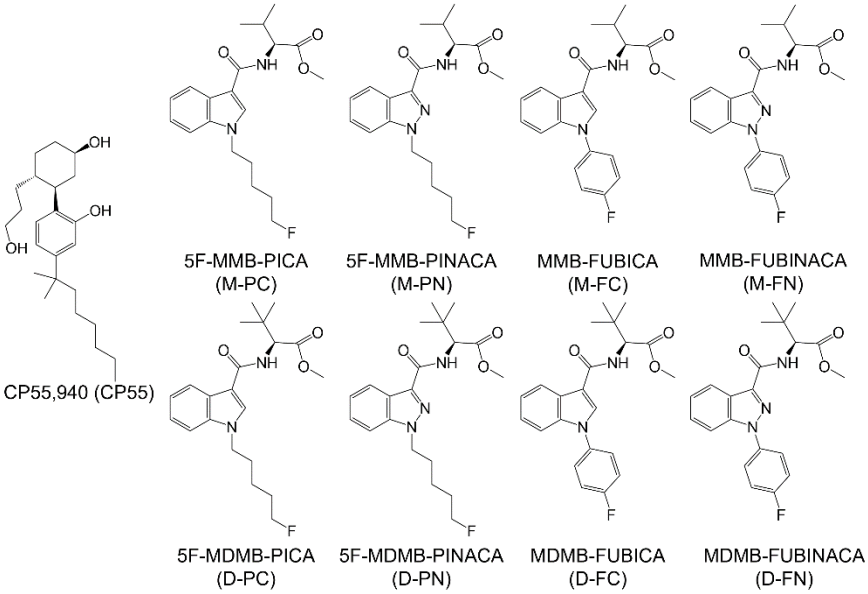

Supplementary Figure 1: Structures of SCRAs used in this study. CP55,940 serves as the reference ligand for all experiments.

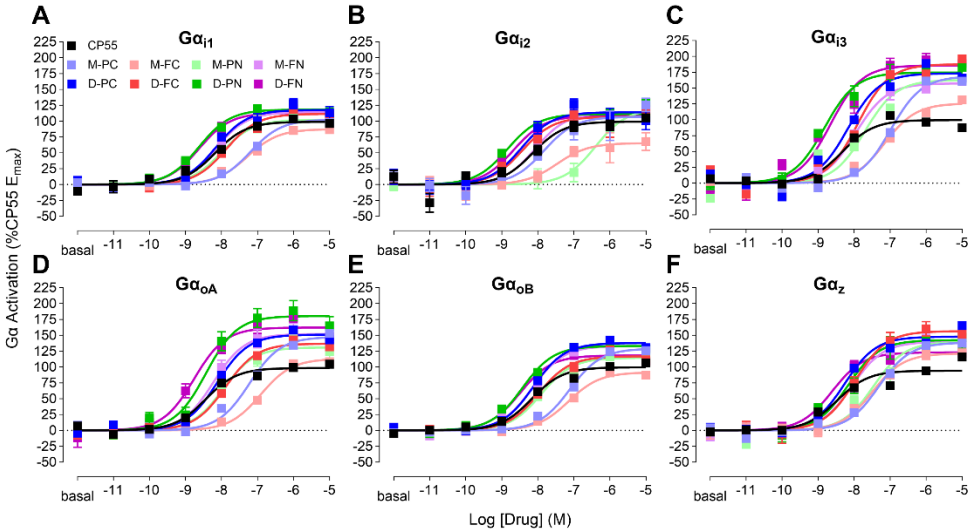

Supplementary Figure 2: Full concentration-response curves of SCRA-mediated G-protein activation. Concentration-response curves of SCRA-induced BRET are plotted as a percentage of CP55 E_{max} for each transducer: $G\alpha_{i1}$ (A), $G\alpha_{i2}$ (B), $G\alpha_{i3}$ (C), $G\alpha_{oA}$ (D), $G\alpha_{oB}$ (E), and $G\alpha_{z}$ (F). Data are presented as means ± SEM of n≥4 experiments.

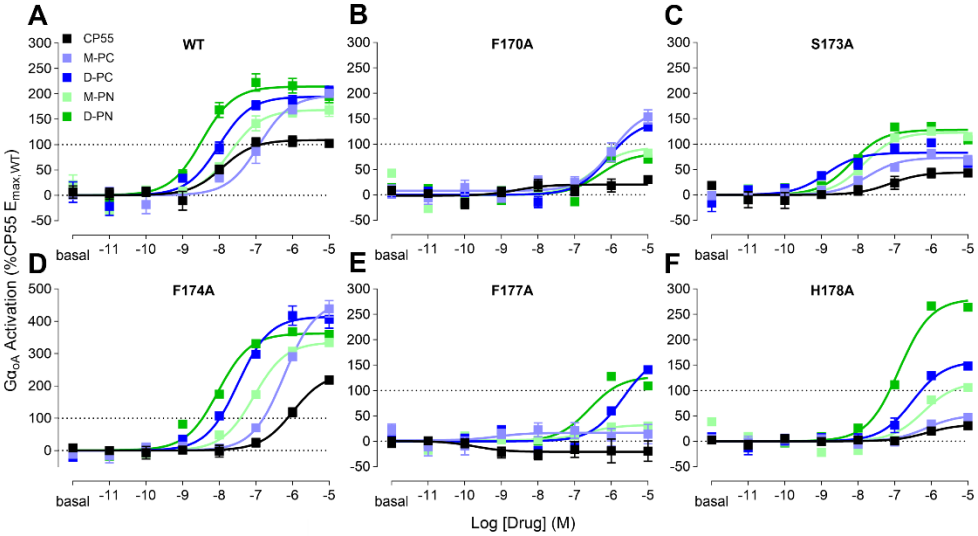

Supplementary Figure 3: CB1R-TM2 mutational analysis of G-protein activation. Through BRET $G\alpha_{oA}$ Activation mode, M-PC, D-PC, M-PN, and D-PN are compared to CP55 in the presence of CB1R with the following TM2 mutations: Wildtype (A), F170A (B), S173A (C), F174A (D), F177A (E), H178A (F). Concentration-response curves of SCRA-induced BRET plotted as a percentage of CP55 $E_{max,WT}$. Data presented as means ± SEM of n=4 experiments.

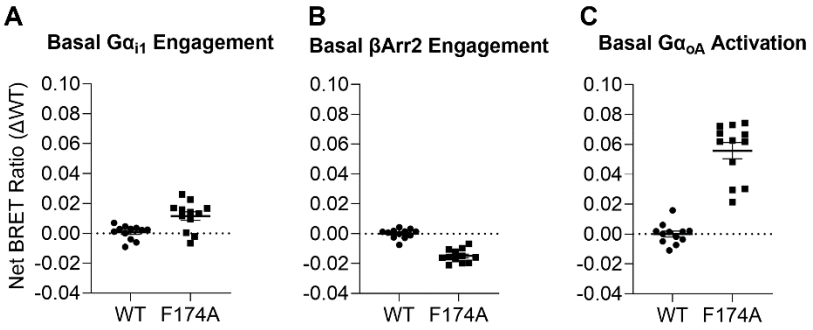

Supplementary Figure 4: Net BRET Ratios of CB1R F174A in different BRET modes. Calculated basal BRET ratios for CB1R F174A are subtracted from basal BRET ratios of wildtype CB1R for $G\alpha_{i1}$ Engagement (A), βArr2 Engagement (B), and $G\alpha_{oA}$ Activation (C) BRET assay modes. Data presented as means ± SEM of n=4 experiments.

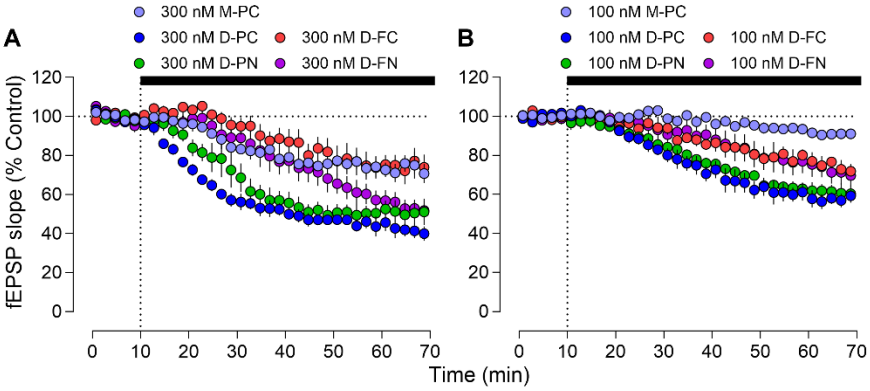

Supplementary Figure 5: Perfusion of SCRAs at lower concentrations in *ex vivo* slice electrophysiology. Field extracellular postsynaptic potentials (fEPSPs) were recorded every 30 seconds in the CA1 hippocampus during SCRA perfusion. After 10 minutes of baseline, SCRAs were perfused for 60 minutes at 300 nM (A) or 100 nM (B). (N≥4 mice; n≥4 recordings; means ± SEM).

Supplementary Table 1: CB1R-TM2 Mutational Analysis with SCRA Head Moiety ($G\alpha_{oA}$ Activation)

	WT		F170A		S173A		F174A		F177A		H178A	
	E_{max} (% CP55,WT)	pEC_{50} (M)	E_{max} (% CP55,WT)	pEC_{50} (M)	E_{max} (% CP55,WT)	pEC_{50} (M)	E_{max} (% CP55,WT)	pEC_{50} (M)	E_{max} (% CP55,WT)	pEC_{50} (M)	E_{max} (% CP55,WT)	pEC_{50} (M)
CP55	100.0 ± 7.03	7.92 ± 0.19	30.3 ± 6.76	N.D.	44.2 ± 8.79*	7.13 ± 0.49	240.1 ± 17.46*	5.99 ± 0.12*	-19.5 ± 19.90	N.D.	33.4 ± 7.10*	6.12 ± 0.38
M-PC	197.3 ± 6.43*	7.91 ± 0.11	168.7 ± 18.23*	5.97 ± 0.19*	73.1 ± 5.06	7.73 ± 0.20	463.9 ± 17.87*	6.23 ± 0.07*	13.9 ± 18.99	N.D.	51.8 ± 8.80	6.14 ± 0.31*
D-PC	194.6 ± 8.38*	8.02 ± 0.14	146.4 ± 10.13	6.08 ± 0.12*	83.0 ± 5.14	8.88 ± 0.22	414.5 ± 11.50*	7.49 ± 0.08	171.7 ± 15.06*	5.67 ± 0.13*	157.8 ± 10.35*	6.51 ± 0.15
M-PN	168.5 ± 8.18*	7.71 ± 0.14	93.5 ± 21.15	6.49 ± 0.50	122.7 ± 9.87	7.84 ± 0.23	335.1 ± 9.12*	7.05 ± 0.07	30.4 ± 11.10	N.D.	116.3 ± 15.57	6.22 ± 0.26*
D-PN	214.6 ± 7.70*	8.48 ± 0.12	82.1 ± 14.29	6.3 ± 0.35*	128.0 ± 7.42	8.17 ± 0.18	362.5 ± 9.54*	8.04 ± 0.08	127.8 ± 14.87	6.6 ± 0.26	280.8 ± 9.83*	6.88 ± 0.08

Data analyzed by one-way ANOVA followed by post-hoc Dunnett test. Data presented as means ± SEM. Significance of * represents $p<0.05$ compared to CP55 E_{max}, pEC_{50} of the wildtype construct. For concentration-response curves with a low potency shift and/or low E_{max} the pEC_{50} was not determined (N.D.) and the E_{max} shown is the effect at the maximum concentration tested (10 μM).